A&A 404, L47–L50 (2003)
DOI: 10.1051/0004-6361:20030670

Astronomy & Astrophysics

Remote diagnostic of the solar-cycle-induced heliospheric interface variation using energetic neutral atoms

K. Scherer and H.-J. Fahr

Institut für Astrophysik und Extraterrestrische Forschung, Universität Bonn, Auf dem Hügel 71, 53121 Bonn, Germany

Received 19 March 2003 / Accepted 28 April 2003

Abstract. The region of perturbed plasma flows between the supersonic solar wind and the supersonic interstellar plasma is generally called the heliospheric interface. This extended plasma region at the boundary of the heliosphere, though theoretically thoroughly studied and revealed as strongly time-variable during the solar activity cycle, is up to the present not accessible by direct or remote observations. Here we emphasize the possibility to remotely investigate this time-variable region by imaging it through energetic neutral atoms. We calculate the time-dependent distribution function of keV-energetic neutral H-atoms originating as products of charge exchange reactions between H-atoms and protons in the interface region. By carrying out line-of sight integrations of time-variable spectral sources of energetic neutral H-atoms we estimate their fluxes for an earth-bound detector as function of time within the solar activity cycle. Our predictions can directly be taken as a basis for the interpretation of planned heliospheric ENA-measurements upcoming in the near future.

Key words. outer heliosphere – solar cycle variation – ENA flux

1. Introduction

Since decades now the location and geometry of the solar wind termination shock and the downstream interface configuration has been subject of intensive theoretical investigations (for a review see Zank 1999). Nevertheless, up to now neither signatures of the shock structure nor of the interface plasma could yet be identified by the distant NASA spaceprobes. Meanwhile not only the location but even more the structure of this shock have become objects of prime interest, since the multi-fluid character of this shock transition was clearly recognized (Zank et al. 1993; Chalov & Fahr 1994, 1995, 1997; LeRoux & Fichtner 1997; Kausch & Fahr 1997; Fahr et al. 2000). The transition properties at the multifluid shock essentially determine the downstream plasma properties which, on the other hand, are practically undefined until now. Though there are many open questions left concerning the basic multifluid interaction processes, meanwhile the global heliospheric interface structures have been modeled by multifluid counterflow simulations as published by Fahr et al. (2000), Fahr (2000), or Scherer et al. (2002).

Since many open problems are outstanding in this field, any form of a helpful diagnostic of these structures will be highly appreciated by the science community. Concerning this fact, already in the recent past the method of an "energetic neutral atom" – imaging (ENA-imaging) has been proposed in the literature for the remote study of planets, comets and of outer heliospheric plasma structures (see Roelof 1987, 1992; Gruntman 1992, 1997; Hsieh & Gruntman 1993; Williams et al. 1992; Barabash et al. 1995; Dubinin & Lundin 1995; Czechowski & Grzedzielski 1998; Scime et al. 1994; Funsten et al. 1994; Gruntman et al. 2001). Since the ENA detection technique in recent years has made important progresses, an increasing number of ambitions are presently coming up to carry out an ENA imaging of heliospheric structures. Meanwhile, however, a severe complication for the use of this technique has been emphasized in recent works by Scherer & Fahr (2002, 2003) who have treated the heliospheric multifluid interface under the action of solar-cycle induced variations of the solar wind momentum flow. As shown by these authors complicated time-dependent reactions of the whole interface system result as a consequence of the solar-cycle trigger which, when not taken into account, leads to erroneous interpretations of heliospheric ENA images. In the following, we present, as a guide for upcoming ENA observers, results on theoretically calculated heliospheric ENA fluxes originating in a time-dependent heliospheric interface.

2. Theoretical approach and calculations

As basis of our ENA calculations we use the well tested five-fluid interaction model first published by Fahr et al. (2000) describing the solar wind – interstellar medium counterflow configuration by a consistent dynamic and thermodynamic interaction of the following five fluids: protons, H-atoms, H-pick-up ions, H-anomalous and galactic cosmic rays. This model which was originally run with stationary solar and

Send offprint requests to: K. Scherer,
e-mail: kscherer@astro.uni-bonn.de

interstellar boundary conditions most recently was further developed by Scherer & Fahr (2002, 2003) to take into account non-stationary solar wind conditions which simulate typical solar cycle periodic variations. As result of this time-dependent modeling it was shown, how the hydrodynamic properties of the above mentioned five fluids vary in time and space during consecutive solar activity cycles. Here we make use of the time-dependent local properties of H-atoms and protons to calculate local H-ENA spectral production rates $\Psi(\boldsymbol{r}, \boldsymbol{v}, \tau)$ in the heliospheric interface region.

These local production rates are given by:

$$\Psi(\boldsymbol{r}, \boldsymbol{v}, \tau) = \left| n_{\rm p}\, f_{\rm p}(\boldsymbol{v}) n_{\rm H} \sigma_{\rm ex}(v_{\rm rel}) v_{\rm rel} \right|_{\boldsymbol{r},\tau} \quad (1)$$

where $n_{\rm p}$ and $n_{\rm H}$ are the local proton and H-atom densities, respectively, $f_{\rm p}(\boldsymbol{v})$ is the proton velocity distribution function, $\sigma_{\rm ex}$ is the charge exchange cross section, and $v_{\rm rel}$ is the mean relative velocity between H-atoms and protons of velocity $\boldsymbol{v}$. Within the hydrodynamic multifluid model the proton distribution function is given by a shifted Maxwellian in the form:

$$f_{\rm p}(\boldsymbol{r}, \boldsymbol{v}, \tau) = \left(\frac{2\pi K T_{\rm p}}{m}\right)^{-3/2} \exp\left[-\frac{m}{2KT_{\rm p}}(\boldsymbol{V}_{\rm p} - \boldsymbol{v})^2\right] \quad (2)$$

where $T_{\rm p}$ and $\boldsymbol{V}_{\rm p}$ are the time-dependent local proton bulk velocity and temperature, respectively (given by Scherer & Fahr 2002). The mean relative velocity is calculated with the following expression (see Ripken & Fahr 1983):

$$v_{\rm rel} = \sqrt{\frac{2KT_{\rm H}}{m}}\left[\frac{1}{\sqrt{\pi}}\exp\left[-w_{\rm H}^2\right] + w_{\rm H}\left(1 + \frac{1}{2w_{\rm H}}\right)\mathrm{erf}(w_{\rm H})\right] \quad (3)$$

where $T_{\rm H}$ is the H-atom temperature, and $w_{\rm H}$ is defined as:

$$w_{\rm H} = \sqrt{v^2 + V_{\rm H}^2 - 2vV_{\rm H}\cos\vartheta_{\rm p,H}}\sqrt{\frac{m}{2KT_{\rm H}}} \quad (4)$$

where $\cos\vartheta_{\rm p,H}$ is the cosine of the angle between the H-atom bulk flow $\boldsymbol{V}_{\rm H}$ and the individual proton velocity $\boldsymbol{v}$. The charge exchange cross section is adopted here according to Maher & Tinsley (1977):

$$\sigma_{\rm ex}(v_{\rm rel}) = \left[1.64. \times 10^{-7} - 1.6 \times 10^{-8}\log(\overline{v_{\rm rel}})\right]^2 \quad (5)$$

where $\overline{v_{\rm rel}}$ is the speed in units of $[\mathrm{cm\,s^{-1}}]$.

Selecting now a special line of sight with its origin at the Earth (i.e. practically identical with that to the Sun) and with an inclination of Θ with respect to the local interstellar medium (LISM) wind axis, that requires protons of a special inclination $\cos\vartheta_{\rm pp}$ with respect to the proton bulk velocity $\boldsymbol{V}_{\rm p}$ in order to gain appropriate H-atoms which after creation fly into the right direction along this line of sight to finally reach the Earth. The Maxwellian probability weight of such protons is determined by the exponential argument:

$$v^2(\Theta) = (\boldsymbol{V}_{\rm p} - \boldsymbol{v})^2 = V_{\rm p}^2 + v^2 \pm 2vV_{\rm p}\cos\vartheta_{\rm pp} \quad (6)$$

where $\cos\vartheta_{\rm pp}$, in order to meet the line of sight (LOS) – condition, has to fulfill the following condition:

$$\cos\vartheta_{\rm pp} = \cos\Theta\frac{V_{{\rm p},z}}{V_{\rm p}} - \sin\Theta\frac{V_{{\rm p},x}}{V_{\rm p}} \quad (7)$$

where $v_{{\rm p},z}$ and $v_{{\rm p},x}$ are the components of $\boldsymbol{v}_{\rm p}$ perpendicular and parallel to the inflow axis, respectivley.

Now the LOS-integrated H-ENA production yielding H-atoms that move with the velocity $v(\Theta)$ along the line of sight up to their arrival at Earth at time t is given by:

$$\Phi_{\rm ENA}(v(\Theta), \Theta, t) = \int_{\rm IB}^{\rm BS}\Psi(\boldsymbol{r}, \boldsymbol{v}, \tau)\mathrm{d}s = \int_{\rm IB}^{\rm BS}\left| n_{\rm p}\, f_{\rm p}(\boldsymbol{v}(\Theta)) n_{\rm H}\sigma_{\rm ex}(v_{\rm rel}) v_{\rm rel}\right|_{\boldsymbol{r},\tau}\mathrm{d}s \quad (8)$$

where the retarded time $\tau = t - s/v(\Theta)$ gives the time of flight for an ENA particle of velocity $v(\Theta)$ along the distance s. Because the production rate of the ENAs inside the termination shock is negligible, the inner integration boundary (IB) of the model (5 AU) is taken. The outer integration boundary is the bow shock (BS), beyond which the ENA production is again negligible. The maximum time of flight is then given by $\tau_{\rm max} = L_{\rm max}/v(\Theta)$, where $L_{\rm max}$ is either the BS-distance or a cut-off distance in the tail region (see below).

In the following we display results of ENA fluxes $\Phi_{\rm ENA}(v(\Theta), \Theta, t)$ in units of atoms/cm^2/s/ster obtained at Earth for different times t. We thereby calculate differential ENA fluxes $\Delta\Phi_{\rm ENA}(v(\Theta), \Theta, t)$ within different energy ranges $E_i \le \Delta E_{i,j} \le E_j$ given by:

$$\frac{1}{2}m\left[v_i^2(\Theta)\right] \le \Delta E_{i,j} \le \frac{1}{2}m\left[v_j^2(\Theta)\right] \quad (9)$$

which are shown in Fig. 1.

In the tail region the particle may originate within distances of $L_{\rm max} = 1500$ AU away from the Sun (Earth), if that distance is smaller than that to the bow shock, and ENA's still survive on their passage to the detector. Beyond 1500 AU no further production is assumed. The reason is, that in the tail region from the side warm neutral hydrogen atoms can penetrate and slowly dissolve the region dominated by solar wind ions, and finally the heliospheric tail plasma is completely adapted to the interstellar medium flow not producing ENA's, anymore, which can enter the inner solar system. This cut-off distance is assumed to be 1500 AU (see Jäger & Fahr 1998). The penetration of the supersonic interstellar hydrogen into the tail region is a kinetic process and cannot accurately be handled with the 5-fluid hydrodynamic model.

3. Discussion of the results

As it is evident from Figs. 1a through 1e the resulting H-ENA fluxes at low energies, say between 0.2 keV $\le E \le$ 1.5 keV are strongly peaking in the downwind direction, i.e. into the direction of the heliospheric tail. But it is also clearly visible that both the absolute magnitude of the spectral fluxes and the upwind/downwind anisotropy is substantially varying with the time t of the observation during the solar activity cycle. At higher spectral energies, ≥2.5 keV, the H-ENA fluxes, as shown in Figs. 1f through i, only show distinct upwind/downwind anisotropies for a fraction of the solar activity cycle (about one third), whereas at observation times t associated with later phases of the cycle, the degree of anisotropy becomes less and

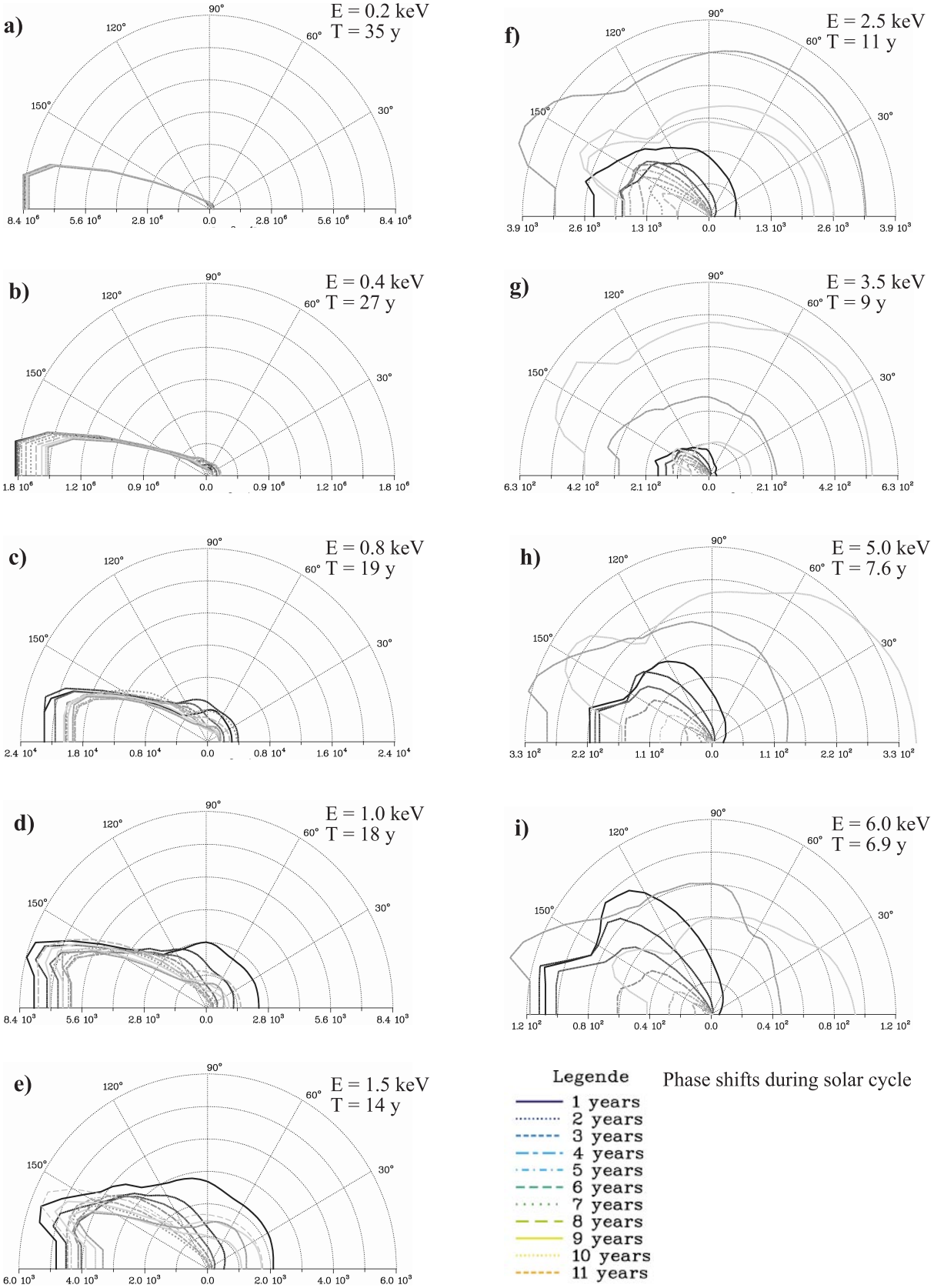

Fig. 1. ENA flux for different energy ranges given in units atoms/cm^2/s/ster. The mean kinetic energy of the neutral H-atoms and the maximm time of flight are indicated at the right top side of each polar plot. In the lower right corner the phase delay for the event time of the measurments is indicated starting at solar minimum conditions. The energy increases from top to bottom, and from left to right. The energy intervals are listed in Table 1.

Table 1. Energy intervals and time of flight, i.e. the maximum travel time taken into account, so that particles from 1500 AU with a given mean energy can reach the detector.

see Fig. 1	mean	lower	upper	max. time of flight [years]
	kinetic energy [keV]			
a)	0.2	0.1	0.3	35.0
b)	0.4	0.3	0.6	27.0
c)	0.8	0.6	0.9	19.0
d)	1.0	0.9	1.2	18.0
e)	1.5	1.2	2.0	14.0
f)	2.5	2.0	3.0	11.0
g)	3.5	3.0	4.7	9.0
h)	5.0	4.7	5.5	7.6
i)	6.0	5.5	10.0	6.9

less pronounced and finally even is reversed. Also the variability – with time during the solar cycle – of the absolute flux intensities at these higher energies is much more pronounced. At energies of about 100 keV, which are observed from the tail region by Czechowski et al. (2001), the fluxes in our model are less than 10^{-20} cm^{-2} s^{-1}, which shows that for this high energy range the above described production mechanism does not work.

The reason for the above described strange behavior of ENAs between 2 keV $\leq E \leq$ 10 keV, is that for the higher energies the time of flight (see Fig. 1) become smaller and then the density waves of protons and hydrogen propagating in the outer heliosphere are no longer smeared out. Thus the observation pattern, as represented in Figs. 1f through i reveals the actual situation in the outer heliosphere, which due to propagation effects and to the heliospheric memory (Scherer & Fahr 2002) is much different from that observed inside the termination shock for the actual solar activity cycle.

Additionally, for energies below 2 keV the passage time close to the Sun (say, inside 5 AU) is about days to weeks and therefore, one should take into account losses of the neutral atoms by solar photoionization and charge exchange processes with the solar wind. These effects are not modeled here. There are, however, of minor importance (Gruntman et al. 2001). For the higher energetic neutral atoms the ionization rates are negligible and, hence, need not be taken into account.

To profitably use these flux patterns and their variabilities as diagnostic tool to determine, on the basis of ENA observations, properties of the heliospheric interface structures, one needs to carefully test the theoretical sensitivity of the properties of these ENA fluxes to a change of the interstellar parameters, like the LISM density, temperature and bulk velocity. The question whether or not there is at all an outer bow shock may for the first time then find an answer.

References

Barabash, S., Lundin, R., Zarnowiecki, T., & Grzedzielski, S. 1995, Adv. Space Res., 16, 81

Chalov, S. V., & Fahr, H. J. 1994, A&A, 288, 973

Chalov, S. V., & Fahr, H. J. 1995, Plan. Space Sci., 43, 1035

Chalov, S. V., & Fahr, H. J. 1997, A&A, 326, 860

Czechowski, A., & Grzedzielski, S. 1998, Geophys. Res. Lett., 25, 1855

Czechowski, A., Fichtner, H., Grzedzielski, S., et al. 2001, A&A, 368, 622

Dubinin, E., & Lundin, R. 1995, Adv. Space Res., 16, 75

Fahr, H. J. 2000, Ap&SS, 274, 35

Fahr, H. J., Kausch, T., & Scherer, H. 2000, A&A 357, 268

Funsten, H. O., McComas, D. J., & Scime, E. E. 1994, Opt. Eng., 33, 342

Gruntman, M. A. 1992, Plan. Space Sci., 40, 439

Gruntman, M. A. 1997, Rev. Sci. Instruments, 65, 758

Gruntman, M., Roelof, E. C., Mitchell, D. G., et al. 2001, J. Geophys. Res. 106, 15767

Hsieh, K. C., & Gruntman, M. A. 1993, Adv. Space Res., 13(6), 131

Jäger, S., & Fahr, H. J. 1998, Sol. Phys., 178, 193

Kausch, T., & Fahr, H. J. 1997, A&A, 325, 828

LeRoux, J. A., & Fichtner, H. 1997, J. Geophys. Res., 102, 17365

Maher, L. J., & Tinsley, B. A. 1977, J. Geophys. Res. 82, 689

Ripken, H. W., & Fahr, H. J. 1983, A&A, 122, 181

Roelof, E. C. 1987, Geophys. Res. Lett., 14, 652

Roelof, E. C. 1992, in Solar Wind Seven, ed. E. Marsch, & R. Schwenn (Pergamon Press), 385

Scherer, K., & Fahr, H. J. 2002, Geophys. Res. Lett. 29, DOI: 10.1029/2002GL016073

Scherer, K., & Fahr, H. J. 2003, Ann. Geophys., accepted

Scherer, K., Fichtner, H., & Stawicki, O. 2002, J. Atmos. Sol. Terrestr. Sci., 64, 795

Scime, E. E., Funsten, H. O., McComas, D. J., Moore, K. R., & Gruntman, M. A. 1994, Opt. Eng., 33, 357

Williams, D. J., Roelof, E. C., & Mitchell, D. G. 1992, Rev. Geophys. Space Phys., 30, 183

Zank, G. P., Webb, G. M., & Donohue, D. J. 1993, ApJ, 406, 67

Zank, G. P. 1999, Space Sci. Rev., 89, 413